Modeling and Quantification of the Protective Effect of Shelterbelts Against Wind Erosion in Vineyards of Mendoza, Argentina

RODOLFO DEMATTE[1,2], JOSEFINA HUESPE[1]
[1]Unidad Investigativa de Epistemología, Lógica y Ciencias Básicas. Grupo IEMI,
Universidad Tecnológica Nacional Facultad Regional Mendoza,
Coronel Rodríguez 273, Ciudad – Capital (M5500) Mendoza,
ARGENTINA

[2]Instituto de Energías Naturales Renovables. CENIIT. SECyT,
Universidad Nacional de La Rioja,
Av. Luis Vernet 1000, La Rioja – Capital (5300) La Rioja,
ARGENTINA

Abstract: - Wind erosion is a critical soil degradation process affecting 77% of Mendoza, Argentina. This study quantifies the 'shelter effect' of forest belts in San Rafael vineyards using Computational Fluid Dynamics (CFD). Employing the DPMFoam solver in OpenFOAM, a two-phase air-sediment flow was modeled within a 3D domain at a 1:100 scale. The simulation utilized a coupled Euler-Lagrange approach, solving RANS equations with the k-ϵ turbulence model to track particle transport (density: 2600 kg/m³). Two scenarios were evaluated under a constant wind speed of 10 m/s: an unprotected vineyard and one shielded by a triple-row forest barrier with 28.26% optical porosity. By maintaining Stokes Number (Stk) similarity, the model ensured a realistic representation of particle inertia. Results indicate that shelterbelts create a significant leeward velocity reduction zone, facilitating sediment deposition and retaining 4.95% of total particles. In contrast, retention in the unprotected scenario was negligible. These findings validate CFD as a robust tool for agroforestry design and confirm that triple-row shelterbelts are an effective strategy for soil conservation in vulnerable viticultural regions.

Key-Words: - Wind erosion, shelter effect, Mendoza, CFD, shelterbelts, Quantification.

Received: January 4, 2026. Revised: March 11, 2026. Accepted: June 28, 2026. Published: September 4, 2026.

1 Introduction

Wind erosion is a primary driver of soil degradation in arid and semi-arid regions, affecting approximately 77% of the territory in Mendoza [1], Argentina. In areas like San Rafael, this phenomenon not only compromises soil fertility by removing nutrient-rich topsoil but also causes direct physical damage to high-value crops such as vineyards. Despite the historical use of forest shelterbelts, there is a critical need for quantitative data to evaluate their aerodynamic efficiency. This study addresses this gap by employing Computational Fluid Dynamics (CFD) to model the interaction between wind-borne particles and complex 3D vegetation structures. By using the DPMFoam solver in OpenFOAM, we simulate the coupled air-sediment flow to quantify the protective effect of these barriers, providing a scientific basis for optimizing agricultural protection in the region.

Several studies agree that soil wind erosion represents one of the main environmental problems in arid and semi-arid regions [2], [3], [4], and even in sub-humid areas [5]. This phenomenon has significant environmental repercussions, as it affects air quality, deteriorates visibility [4], [6], and generates adverse effects on both public health [7] and biodiversity [8]. Soil erosion exacerbates the effects of climate change, diminishes livelihoods by reducing both the quantity and quality of food produced, affects water supply, and causes the degradation of natural ecosystems. Soil depletion also intensifies the effects of meteorological phenomena, increasing the frequency and intensity of droughts and floods. Furthermore, soil erosion indirectly affects urban infrastructure, urban environments, and the quality of life of inhabitants, [9]. The study of wind erosion has gained importance due to climate change, [2], [8]. It represents a significant risk to agricultural lands despite numerous mitigation strategies employed for its control, [10]. The movement of sand grains in the air has been widely studied, as it constitutes the main external agent in the formation of aeolian landforms and the erosion of agricultural fields, [11].

Physically, wind erosion is described as a gas-solid two-phase flow (air and sand), influenced by wind speed, particle size within the dust cloud, and existing obstacles, [2], [10]. Regarding the dynamics of wind erosion (WE), it is fundamental to understand the interaction between the wind and the soil surface, [2]. In agricultural areas, environmental settings have been transformed by human activities, creating new conditions for soil development and generating negative side effects such as salinization, piping, and erosion. Consequently, the mitigation of these processes is a priority in environmental management and sustainable land-use programs, [12].

1.1 Mitigation Strategies: Influence of the Shelter Effect on Wind Erosion Reduction

As a mitigation measure, the use of forest shelterbelts is common in agriculture to reduce the effects of wind. When the flow approaches a shelterbelt, part of the air passes through the barrier, while the rest is diverted around its ends or lifted above it, [13]. This aerodynamic behavior creates a protected zone downwind, known in specialized literature as the "shelter effect", [14], [15]. The reduction of wind speed within this protected zone modifies turbulent transport processes and alters the local microclimate, [15], 16]. This effect is vital for the health and yield of crops, specifically in vineyards [17], as it reduces mechanical stress on plants and minimizes the risk of physical damage and soil erosion.

1.2 Wind Erosion in the Province of Mendoza: Geographical and Climatic Context

Regarding the distribution of wind erosion in Mendoza, data from the cartography developed by [1] were analyzed, classifying erosion severity across different regions of the country. Consistent results are shown in the cartographic products, [18].

By overlaying this information with the viticultural regional map of Mendoza, it was observed that in the southern area—corresponding to the departments of San Rafael and General Alvear—wind erosion levels vary between light and moderate. However, toward the eastern sector of San Rafael and the department of General Alvear, these levels intensify, reaching categories of severe or grave erosion (Figure 1). Building upon the findings of previous research [19], where different forest configurations were analyzed to identify the most effective windbreak design, this study selects the most optimal shelterbelt arrangement for the 'shelter effect' in the San Rafael region. Moving beyond simple wind speed reduction, the current work advances by specifically evaluating the particle retention efficiency of this optimal triple-row configuration, providing a quantitative assessment of its capacity to mitigate physical sediment transport through a 1:100 scale DPM simulation.

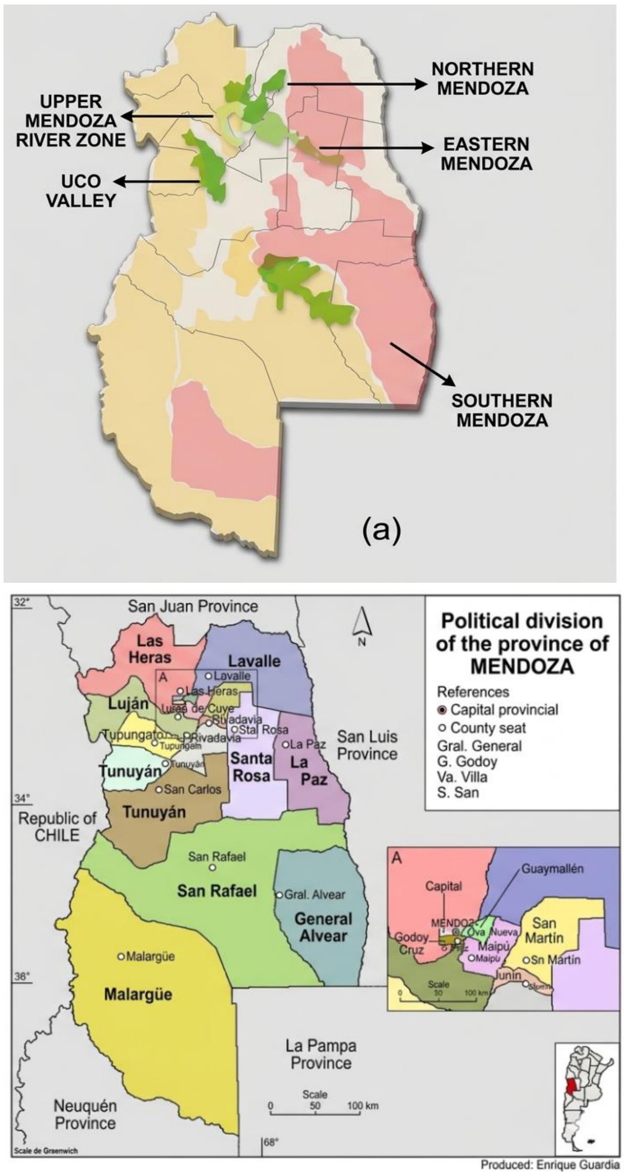

Fig. 1: (a) Wind erosion levels in the province of Mendoza

Source: Own elaboration based on data from [1] (b) Mendoza Province. Source: Enrique Guardia, CC BY 3.0, via Wikimedia Commons.

1.3 Objective

The objective of this study is to analyze and quantify, through numerical simulations, the protective effect of forest shelterbelts against wind erosion, evaluating their efficiency in retaining wind-borne particles.

2 Materials and Methods

Numerical CFD simulations were developed using OpenFOAM V8, employing the DPMFoam solver. This solver allows for the modeling of turbulent flows and discrete particle transport within a coupled multiphase environment, [20]. DPMFoam is a transient Eulerian-Lagrangian solver that treats the fluid phase as a continuum and the solid phase as discrete. It accounts for the effect of the particle volume fraction on the continuous phase, making it ideal for dense particle flows. The model is based on four-way coupling, considering fluid-particle interactions, particle-fluid feedback, and inter-particle collisions, which enables a realistic representation of complex multiphase systems. In the coupled model used by DPMFoam, the Lagrangian code calculates particle positions and velocities; this information is then transferred to the Eulerian code. Within the Eulerian framework, particles are located within the continuous domain mesh, and the cell containing the center of each particle is identified. Subsequently, the particle volume fraction within each cell is calculated. Based on the initial velocities of both the fluid and particles, as well as the calculated volume fraction, fluid-particle interaction forces (such as drag and lift) are determined, and the momentum exchange terms between both phases are assembled. Finally, these forces are returned to the Lagrangian code to update the particle velocity field for the next time step, [21].

The fluid phase dynamics were solved using the Reynolds-Averaged Navier–Stokes (RANS) equations, utilizing the PIMPLE algorithm for the analysis of turbulent Newtonian fluid flow (Table 1). The k-epsilon turbulence model was employed in this study. Initial turbulent kinetic energy (k) and the dissipation rate (epsilon) were established based on typical values reported in the literature for atmospheric flows near ground level, [10].

Furthermore, the fluid-particle interaction process is assumed to occur under an isothermal regime. The calculation is performed by solving a system of ordinary differential equations that accounts for all relevant forces acting on each particle, such as friction, gravity, buoyancy, and pressure forces, [22].

The applications of the DPM model are numerous; in the agricultural industry, this solver can be used to predict the interaction of particles with the fluid and surrounding objects, such as shelterbelts and the specific vineyard cultivation area analyzed, [22].

Table 1. Summary of parameters and numerical model conditions

Parameter	Description
Fluid Type	Newtonian
Turbulent Kinetic Energy (k)	1.5 m^2/s^2
Dissipation Rate (epsilon)	0.03 m^2/s^3
Turbulent Viscosity (nu_t)	Dynamically calculated at each iteration
Flow Velocity	10 m/s
Pressure	Determined by the SIMPLE method
Kinematic Viscosity (nu)	1.5 x 10^{-5} m^2/s^2 (at 20°C)

Source: created by the authors

2.1 Mathematical Framework and Governing Equations

The numerical simulation of the air-sediment interaction follows a coupled Euler-Lagrange approach. The fluid phase (air) is treated as a continuum, while the solid phase (sediment particles) is modeled as a discrete phase.

2.1.1 Fluid Phase Equations

The airflow is governed by the Reynolds-Averaged Navier-Stokes (RANS) equations for an incompressible fluid. The conservation of mass (1) and momentum (2) are expressed as follows:

$$\nabla \cdot \bar{\mathbf{u}} = 0 \tag{1}$$

$$\rho \left(\frac{\partial \bar{\mathbf{u}}}{\partial t} + \bar{\mathbf{u}} \cdot \nabla \bar{\mathbf{u}} \right) = -\nabla \bar{p} + \mu \nabla^2 \bar{\mathbf{u}} + \rho \mathbf{g} + \mathbf{S}_p \tag{2}$$

where $\bar{\mathbf{u}}$ is the mean velocity, $\bar{p}$ is the mean pressure, ρ is the air density, $\mathbf{g}$ is the gravitational acceleration, and $\mathbf{S}_p$ represents the momentum exchange (source term) with the discrete phase (3). To close the system, the standard k-ϵ turbulence model is employed, introducing transport equations for the turbulent kinetic energy (k) (3) and its dissipation rate (ϵ) (3.1)

$$\frac{\partial(\rho k)}{\partial t} + \nabla \cdot (\rho k \mathbf{u}) = \nabla \cdot \left[\left(\mu + \frac{\mu_t}{\sigma_k}\right) \nabla k\right] + G_k - \rho\epsilon \quad (3)$$

$$\frac{\partial(\rho\epsilon)}{\partial t} + \nabla \cdot (\rho \mathbf{u} \epsilon) = \nabla \cdot \left(\left(\mu + \frac{\mu_t}{\sigma_\epsilon}\right) \nabla \epsilon\right) + C_{1\epsilon} \frac{\epsilon}{k} G_k - C_{2\epsilon} \rho \frac{\epsilon^2}{k} \quad (3.1)$$

2.1.2 Particle Dynamics (Lagrangian Frame)

The motion of each individual sediment particle is calculated by integrating the force balance equation (4):

$$m_p \frac{d\mathbf{u}_p}{dt} = \mathbf{F}_D + \mathbf{F}_G \quad (4)$$

where m_p is the particle mass, $\mathbf{F}_G$ Gravitational Force and $\mathbf{u}_p$ is the particle velocity. The drag force $\mathbf{F}_D$ is modeled using the Schiller-Naumann correlation (5), which is valid for particle Reynolds numbers up to 1000 (6):

$$C_D = \frac{24}{Re_p}\left(1 + 0.15 Re_p^{0.687}\right) \quad (5)$$

$$C_D = \begin{cases} \frac{24}{Re_p}\left(1 + 0.15 Re_p^{0.687}\right) & Re_p \le 1000 \\ 0.44 & Re_p > 1000 \end{cases} \quad (6)$$

To calculate this coefficient, the Particle Reynolds Number (Re_p) is defined as:

$$Re_p = \frac{\rho d_p |\mathbf{u} - \mathbf{u}_p|}{\mu} \quad (7)$$

where:
ρ: Air density
d_p: Particle diameter.
u : Fluid velocity.
u_p: Particle velocity
μ: Dynamic viscosity of air.

2.1.3 Similarity and Scaling

To ensure that the 1:100 scale model accurately represents the full-scale phenomenon, the Stokes Number (Stk) is used as the primary similarity criterion (8). It characterizes the behavior of particles suspended in a fluid flow:

$$Stk = \frac{\tau_p \cdot U_o}{L_c} \quad (8)$$

where τ_p is the relaxation time of the particle, U_o is the characteristic velocity (10 m/s), and L_c is the characteristic length (height of the vines). By maintaining $Stk > 1$, the model ensures that particle inertia is sufficient to deviate from fluid streamlines, allowing for a realistic quantification of the "shelter effect" and particle deposition.

To ensure the physical consistency of the 1:100 scale model, dynamic similarity was maintained through the Stokes Number (Stk) and the Reynolds Number (Re). While achieving full Reynolds independence is challenging in scaled models, the simulation was conducted in a fully turbulent regime where the flow patterns become independent of the Reynolds number, thus accurately representing the aerodynamic behavior of the full-scale shelterbelt.

2.1.4 Metrics for Particle Retention

The retention efficiency η is defined to quantify the "shelter effect" of the forest belts:

$$\eta = \left(1 - \frac{\dot{m}_{out}}{\dot{m}_{in}}\right) \times 100$$

where $\dot{m}_{in}$ is the mass flow rate of particles at the inlet and $\dot{m}_{out}$ is the mass flow rate at the outlet.

2.1.5 Mesh Generation

The base mesh was generated using *blockMesh* with a resolution of 2.26 million cells. Subsequently, *snappyHexMesh* was used to refine the mesh and incorporate the complex geometry of the forest shelterbelts, modeled from a .obj file. Up to five levels of refinement were applied to specific surfaces and regions, prioritizing the areas near obstacles where higher flow complexity and pressure gradients are expected, [19].

2.1.6 Geometry Configuration

The physical domain corresponds to a prism 200 m long, 40 m wide, and 40 m high in full scale. For processing efficiency, simulations were performed at a 1/100 scale, maintaining the proportion and relative location of obstacles. The cultivation area consists of a plot measuring 8.7 m by 13.5 m (scaled), with three rows of low-trellis vines (Vitis vinifera), with a plant spacing of 1.2 m and a uniform height of 1.2 m. All plants and supports are represented as impenetrable solids with a no-slip condition.

To evaluate the "shelter effect," the shelterbelt was incorporated 2H upstream of the plot (where H = 6.6 m is the maximum belt height). Two scenarios were developed in SketchUp (Figure 2):

a) Trial 1: Baseline model without a forest barrier (100% optical porosity).
b) Trial 2: Protected model with a triple-row parallel forest shelterbelt (28.26% optical porosity).

Optical Porosity (OP) is defined as the quantitative ratio between the area of open spaces (pores) and the total projected area of the vegetative barrier, measuring its capacity to reduce wind speed, [19], [21], [23].

A grid independence test was performed to ensure that the numerical solutions were not biased by the spatial discretization of the domain. Three levels of refinement (coarse, medium, and fine) were evaluated by comparing leeward velocity profiles and particle concentration patterns. The current mesh, consisting of approximately 1.2 million cells, was selected as it demonstrated a variance of less than 1% compared to the finer mesh. This convergence confirms that the simulation results are independent of the grid density, ensuring the numerical stability and reliability of the model.

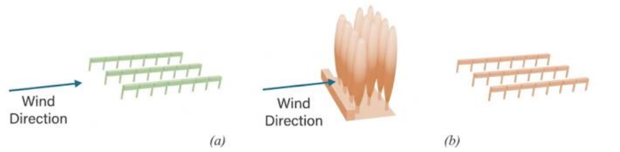

Fig. 2: 3D digital models developed in SketchUp. (a) Trial 1 showing the model without a forest barrier. (b) Trial 2 showing the model equipped with a triple-row parallel forest shelterbelt system. These 3D representations allowed for the construction of realistic geometries for CFD implementation while maintaining consistency with field-measured dimensions and configurations.
Source: generated by the authors using Sketch Up® software.

2.1.7 Boundary and Initial Conditions

Boundary conditions were defined as "walls" for the lateral, top, and bottom faces, while the inlet and outlet allowed for free flow to avoid recirculation, [21]. A "no-slip" condition was applied to all solid surfaces. For turbulence variables, wall functions were employed (kqRWallFunction and epsilonWallFunction), ensuring an accurate representation of the boundary layer.

The numerical resolution utilized the PIMPLE algorithm, which combines PISO and SIMPLE features to enhance stability in transient simulations. Second-order spatial discretization schemes (Gauss linearUpwind) were implemented to ensure numerical accuracy, [19].

2.1.8 Particle Parameterization and Similarity Criteria

The dispersed phase was parameterized based on empirical data from the San Rafael region (Table 2).

Table 2. Physical parameters of particles used in the numerical simulation

Parameter	Description / Value
Number of simulated particles	10,123,140
Average Particle Size (Diameter)	1 x 10^{-4} m
Particle Type	Spherical
Density	2600 kg/m³
Particle Mass	1.3614 x 10^{-9} kg

Source: created by the authors

2.1.9 Initial Conditions and Similarity Criteria

The initial conditions and biophysical parameters of the particles were parameterized based on empirical data from previous studies in the San Rafael region [19] and local granulometric analyses (Table 2).

The physical validity of the 1:100 scaling and the dispersed phase configuration is justified by the following criteria:

- Reynolds Number (Re) Independence: The model ensures a fully turbulent regime (Re > 10,000).
- Stokes Similarity (Stk): As derived in Section 2.1.3, by preserving the actual diameter of the particles (1 x 10^{-4} m) within the scaled domain, the resulting Stokes Number ($Stk > 1$) accurately models the inertia of the solid phase.
- One-way Coupling: Given the low particle volume fraction $\phi = 3.31 \times 10^{-5}$,one-way kinematic coupling is sufficient, where the fluid influences the particles but particle-on-fluid impact is negligible.

The total simulated time was 10 seconds, with a time step of 0.05 seconds, processed across 4 parallel subdomains. Post-processing and visualization were performed using ParaView 5.6.2.

3 Results

This section presents the results from the two analyzed trials, aiming to quantify the particle retention efficiency of the shelterbelt and the vineyard against 10 m/s winds.

The results of the numerical simulation, summarized in Table 3, illustrate the evolution of the dispersed phase over time. At the beginning of the simulation (t=0), a total of 10,246,720 particles are injected into the domain. As the wind flow (10 m/s) develops, the particle count stabilizes, reaching a steady-state equilibrium at t=3 seconds (Figure 3, Appendix). In Trial 1 (Unprotected), the absence of obstacles allows all particles to be transported by the airflow, resulting in 0% retention within the vineyard area. Conversely, in Trial 2 (Shelterbelt), the triple-row forest barrier creates a low-velocity wake zone that promotes sediment deposition. In this scenario, the system maintains a constant retention of 486,340 particles, representing an instantaneous efficiency of 4.95%. While this percentage might appear low in isolation, it represents a significant mitigation effect compared to the unprotected scenario. Furthermore, this value refers to the steady-state concentration; when integrated over the total exposure time, the cumulative mass of sediment prevented from impacting the crop confirms the high protective capacity of the 28.26% optical porosity barrier.

Table 3. Scenario with a triple-row tree and hedge shelterbelt (4-3-4 configuration), 28.26% optical porosity: temporal evolution of retained and removed particles

Time (s)	Scenario	Total Particles	Retention (%)
0	Initial Injection (Both)	10,246,720	100.00%
3	Trial 1 (Unprotected)	0	0.00%
3	Trial 2 (Shelterbelt)	486,340	4.95%

Source: created by the authors

3.1 Protective Shelter Effect on Wind and Particle Distribution

Figure 4 (Appendix) demonstrates how the presence of forest belts modifies the trajectory and concentration of suspended particles, creating low-velocity zones that act as particle capture or retention areas. This dynamic contributes to reducing wind erosion and protects both the soil and the crops. A notable concentration of retained particles is observed in the shelterbelt zone, which acts as a physical barrier capable of reducing wind speed and favoring particle deposition. According to the trials conducted, once the flow reaches a steady-state equilibrium (from t=3), the forest belt maintains a constant retention of 4.95% of the simulated particles (Figure 5). While this percentage represents the instantaneous efficiency under stable conditions, it marks a critical difference compared to the unprotected scenario (Trial 1), where retention is null (0%). This highlights that even with an optical porosity of 28.26%, the triple-row barrier is effective at disrupting the sediment transport layer and promoting the settling of nearly half a million particles that would otherwise impact the vineyard.

Fig. 5: Spatial distribution and particle retention in forest belts and vineyards
Source: generated by the authors using ParaFoam software

4 Conclusion

The results obtained in this study confirm the effectiveness of forest shelterbelts in reducing wind erosion, evidencing a clear "shelter effect" that decreases wind velocity and improves leeward particle retention. These findings are consistent with previous research, such as [19] and [24], which highlighted the importance of height, configuration, and optical porosity in optimizing the protective capacity of vegetative barriers.

The innovative aspect of this research lies in the quantification of the erosion process through Computational Fluid Dynamics (CFD). By using the DPMFoam solver in OpenFOAM, it was possible to model the complex interaction between wind flow, discrete particles, and forest barriers, reproducing conditions that would be difficult to control in the field. This approach allowed for a detailed spatial analysis of the protection zones and the influence of parameters such as the 28.26% optical porosity of the belt.

The comparison between scenarios revealed significant differences. In Trial 1 (Unprotected), particle retention was nearly zero, implying a total loss of sediment in the absence of barriers. In contrast, Trial 2 (Triple-row Shelterbelt) reached a stable steady-state retention of 4.95% from the third second onwards. Although this value represents the instantaneous efficiency under stable flow, it signifies a critical protective threshold compared to the total lack of retention in the unprotected vineyard. The visualization of streamlines confirms that the forest belt generates a low-velocity wake that favors particle deposition, protecting the crop downstream.

4.1 Limitations and Future Work

The present study has limitations that define its scope. First, representing vegetation as impenetrable solids simplifies the intrinsic porosity of foliage;

future work will incorporate porous media models (Darcy-Forchheimer) to refine the description of pressure drops through the canopy. Second, while a uniform velocity profile was used for this initial assessment, subsequent stages will implement a logarithmic gradient to better represent the Atmospheric Boundary Layer (ABL).

Finally, although the RANS k-epsilon model and one-way kinematic coupling ensured statistical convergence for this 1:100 scale analysis, the next phase will transition toward Large Eddy Simulations (LES). This will allow for a more detailed characterization of turbulent vortex structures and sediment transport in prolonged regimes, further optimizing the design of sustainable agroforestry systems in the San Rafael region, Mendoza.

References:

[1] *(text in Spanish)* Casas, R. R., Godagnone, R. E., & de la Fuente, J. C. (2022). Assessment and mapping of water erosion in Argentina (Evaluación y cartografía de la erosión hídrica en la Argentina). *Revista de Investigaciones Científicas de la Universidad de Morón*, *6* (11), [Online]. https://repositorio.unimoron.edu.ar/handle/10.34073/290 (Accessed Date: January 10, 2026).

[2] Miri, A., Dragovich, D., & Dong, Z. (2017). Vegetation morphologic and aerodynamic characteristics reduce aeolian erosion. *Scientific Reports*, *7*(12831), 1-9. https://doi.org/10.1038/s41598-017-13084-x.

[3] Fang, H., Wu, X., Zou, X., & Yang, X. (2018). An Integrated Simulation-Assessment Study for Optimizing Wind Barrier Design. *Agricultural and Forest Meteorology*, *263*, 198–206. https://doi.org/10.1016/j.agrformet.2018.08.018.

[4] Kheirabadi, H., Mahmoodabadi, M., Jalali, V., & Naghavi, H. (2018). Sediment flux, wind erosion, and net erosion influenced by soil bed length, wind velocity and aggregate size distribution. *Geoderma*, *323*, 22-30. https://doi.org/10.1016/j.geoderma.2018.02.042.

[5] Yang, F., Yang, X., Huo, W., Ali, M., Zheng, X., Zhou, C., & He, Q. (2017). A continuously weighing, high frequency sand trap: Wind tunnel and field evaluations. *Geomorphology*, *293*(Part A), 84-92. https://doi.org/10.1016/j.geomorph.2017.04.008.

[6] Sherman, D. (2020). Understanding wind-blown sand: Six vexations. *Geomorphology*, *366*, 107193. https://doi.org/10.1016/j.geomorph.2020.107193.

[7] Bonifacio, H. F., Maghirang, R. G., & Glasgow, L. A. (2014). Numerical simulation of transport of particles emitted from ground-level area source using AERMOD and CFD. *Engineering Applications of Computational Fluid Mechanics*, *8*(4), 488-502. https://doi.org/10.1080/19942060.2014.11015531.

[8] FAO. (2019). *Proceedings of the Global Symposium on Soil Erosion 2019 (GSER19)*. Food and Agriculture Organization of the United Nations, [Online]. http://www.fao.org/3/ca5697en/ca5697en.pdf (Accessed Date: January 10, 2026).

[9] FAO. (2017). *Soil erosion: the greatest challenge for sustainable soil management*. Food and Agriculture Organization of the United Nations, [Online]. https://openknowledge.fao.org/server/api/core/bitstreams/a268e967-a373-4a56-adac-ae1d7ab3567f/content (Accessed Date: January 10, 2026).

[10] Gonzales, H. B., Tatarko, J., Casada, M. E., Maghirang, R. G., Hagen, L. J., & Barden, C. J. (2019). Computational fluid dynamics simulation of airflow through standing vegetation. *Transactions of the ASABE*, *62*(6), 1713–1722. https://doi.org/10.13031/trans.13449.

[11] Fu, J., Yan, S., & Liu, J. (2022). Numerical simulation and wind tunnel test on Aeolian sand transport and settlement with influencing parameters. *Journal of Wind Engineering and Industrial Aerodynamics*, *228*, Article 105074. https://doi.org/10.1016/j.jweia.2022.105074.

[12] Zárate, M., & Mehl, A. (2019). Soils of the Cuyo region. In G. Rubio, R. Lavado, & D. Pereyra (Eds.), *The soils of Argentina* (World Soils Book Series, pp. 135-148). Springer International Publishing. https://doi.org/10.1007/978-3-319-76853-3_9.

[13] Brandle, J. R., Takle, E., & Zhou, X. (2022). Windbreak practices. In *North American agroforestry* (3rd ed., pp. 91–126). American Society of Agronomy. https://doi.org/10.1002/9780891183785.ch5.

[14] He, X., & Shao, Y. (2024). Effect of shelterbelts on wind erosion and dust emission: A numerical study using a high-

resolution atmospheric model. *Journal of Wind Engineering and Industrial Aerodynamics*, *245*, Article 105632. https://doi.org/10.1016/j.jweia.2023.105632.

[15] Zhao, Y., Liu, X., & Li, Y. (2024). Turbulent transport and shelter effect of multiple windbreak systems in arid regions: A CFD approach. *Agricultural and Forest Meteorology*, *346*, Article 109874. https://doi.org/10.1016/j.agrformet.2023.109874.

[16] Wang, H., Takle, E. S., & Shen, J. (2001). Shelterbelts and windbreaks: Mathematical modeling and computer simulations of critical phenomena. *Boundary-Layer Meteorology*, *100*(3), 477–503. https://doi.org/10.1023/A:1019275010070.

[17] Oberschelp, G. P. J., Harrand, L., Mastrandrea, C. A., Salto, C. S., & Flores Palenzona, M. H. (2020). *Cortinas forestales: rompevientos y amortiguadoras de deriva de agroquímicos*. Estación Experimental Agropecuaria Concordia, INTA. https://hdl.handle.net/20.500.12123/21382.

[18] Avecilla, F., Panebianco, J. E., Iturri, L. A., de Oro, L. A., Comas, R. N., & Buschiazzo, D. E. (2023). Dust deposition in agricultural landscapes: Temporal and spatial dynamics along a transect into a natural forest patch. *Aeolian Research, 63–65*, 100887. https://doi.org/10.1016/j.aeolia.2023.100887.

[19] Dematte, R. A., Gandolfo Raso, E., & Huespe, J. (2025). Protection of vineyards from Zonda wind: Evaluation of forest windbreaks. Mendoza, Argentina. *Investigaciones Geográficas*, (*83*), 91–107. https://doi.org/10.14198/INGEO.27853.

[20] Islas, A., Rodríguez-Fernández, A., Betegón, C., Martínez-Pañeda, E., & Pandal, A. (2022). CFD simulations of turbulent dust dispersion in the 20 L vessel using OpenFOAM. *Powder Technology*, *397*, Article 117033. https://doi.org/10.1016/j.powtec.2021.117033.

[21] Fernandes, C., Semyonov, D., Ferrás, L. L., & Nobrega, J. M. (2018). Validation of the CFD-DPM solver DPMFoam in OpenFOAM® through analytical, numerical and experimental comparisons. *Granular Matter*, *20*(4), 1–18. https://doi.org/10.1007/s10035-018-0834-x.

[22] Greenshields, C., & Weller, H. (2022). *Notes on computational fluid dynamics: General principles*. CFD Direct Ltd. ISBN: 978-1-3999-2078-0

[23] Kučera, J., Podhrázská, J., Karásek, P., & Papaj, V. (2020). The effect of windbreak parameters on the wind erosion risk assessment in agricultural landscape. *Journal of Ecological Engineering*, *21*(1), 150-156. https://doi.org/10.12911/22998993/116323.

[24] Judd, M. J., Raupach, M. R., & Finnigan, J. J. (1996). A wind tunnel study of turbulent flow around single and multiple windbreaks, part I: Velocity fields. *Boundary-Layer Meteorology*, *80*(1–2), 127–165. https://doi.org/10.1007/BF00119015.

Contribution of Individual Authors to the Creation of a Scientific Article (Ghostwriting Policy)

All authors contributed equally to all aspects of this work, including simulations, implementation, experiments, and statistical analysis.

Sources of Funding for Research Presented in a Scientific Article or Scientific Article Itself

This work was supported by the Secretary of Postgraduate and Graduates (Secretaría de Posgrado y Graduados) of the National University of La Rioja (UNLaR) through the PROFFDOC 2023 project funding.

Conflict of Interest

The authors have no conflicts of interest to declare that are relevant to the content of this article.

APPENDIX

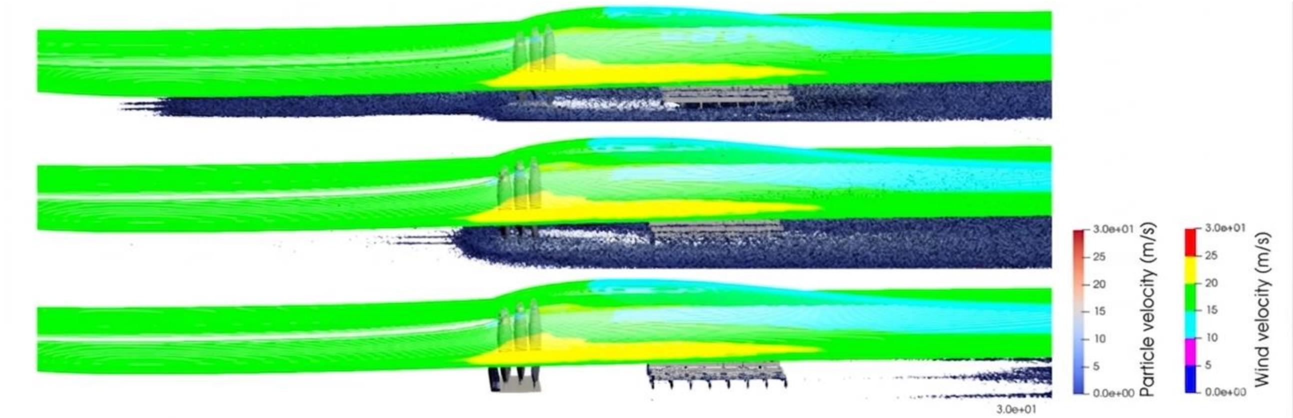

Fig. 3: Wind streamlines and particle distribution, visualizing the shelter effect induced by the forest belt. The model was generated in ParaView from numerical simulation results using the OpenFOAM DPMFoam solver
Source: generated by the authors using ParaFoam software

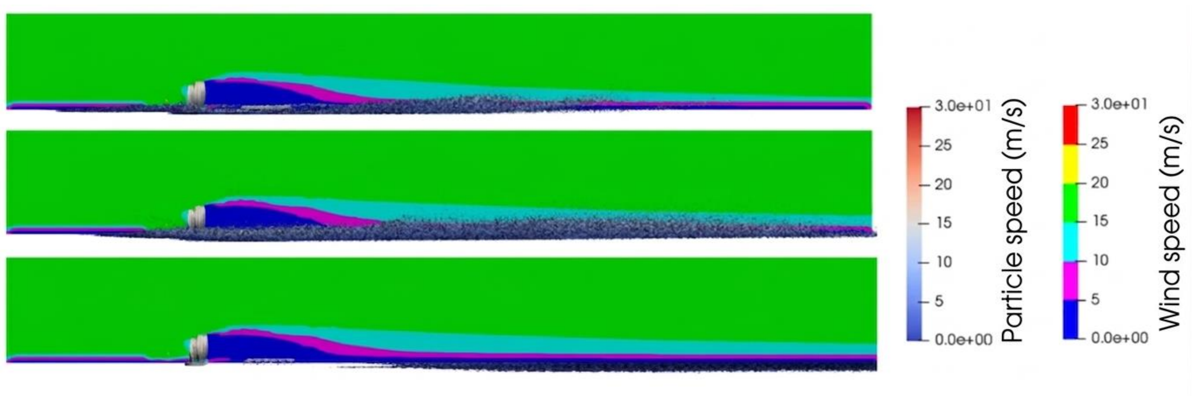

Fig. 4: Protective shelter effect generated by forest belts on wind and particle distribution. Visualization developed in ParaView based on numerical simulation results using the OpenFOAM DPMFoam solver
Source: generated by the authors using ParaFoam software